

Quantum dot self consistent electronic structure and the Coulomb blockade

M. Stopa

RIKEN (The Institute of Physical and Chemical Research)

2-1, Hirosawa, Wako-Shi

Saitama 351-01, Japan

e-mail stopa@sisyphus.riken.go.jp

(March 12, 2018)

We employ density functional theory to calculate the self consistent electronic structure, free energy and linear source-drain conductance of a lateral semiconductor quantum dot patterned via surface gates on the 2DEG formed at the interface of a $GaAs - AlGaAs$ heterostructure. The Schrödinger equation is reduced from 3D to multi-component 2D and solved via an eigenfunction expansion in the dot. This permits the solution of the electronic structure for dot electron number $N \sim 100$. We present details of our derivation of the total dot-lead-gates interacting free energy in terms of the electronic structure results, which is free of capacitance parameters. Statistical properties of the dot level spacings and connection coefficients to the leads are computed in the presence of varying degrees of order in the donor layer. Based on the self-consistently computed free energy as a function of gate voltages, V_i , and N , we modify the semi-classical expression for the tunneling conductance as a function of gate voltage through the dot in the linear source-drain, Coulomb blockade regime. Among the many results presented, we demonstrate the existence of a shell structure in the dot levels which (a) results in envelope modulation of Coulomb oscillation peak heights, (b) which influences the dot capacitances and should be observable in terms of variations in the activation energy for conductance in a Coulomb oscillation minimum, and (c) which possibly contributes to departure of recent experimental results from the predictions of random matrix theory.

PACS numbers: 73.20.Dx, 73.40.Gk, 73.50.Jt

I. INTRODUCTION

Study of the Coulomb blockade and charging effects in the transport properties of semiconductor systems is peculiarly suitable to investigation through self-consistent electronic structure techniques. While the orthodox theory¹, in parameterizing the energy of the system in terms of capacitances, is strongly applicable to metal systems, the much larger ratio of Fermi wavelength to system size, λ_F/L , in mesoscopic semiconductor devices, requires investigation of the interplay of quantum mechanics and charging.

In the first step beyond the orthodox theory, the “constant interaction” model of the Coulomb blockade supplemented the capacitance parameters, which were retained to characterize the gross electrostatic contributions to the energy, with non-interacting quantum levels of the dots and leads of the mesoscopic device^{2,3}. This theory was successful in explaining some of the fundamental features, specifically the periodicity, of Coulomb oscillations in the conductance of a source-dot-drain-gate system with varying gate voltage. Other effects, however, such as variations in oscillation amplitudes, were not explained.

In this paper we employ density functional (DF) theory to compute the self-consistently changing effective single particle levels of a lateral $GaAs - AlGaAs$ quantum dot, as a function of gate voltages, temperature T , and dot electron number N ⁴. We also compute the total system free energy from the results of the self-consistent calculation. We are then able to calculate the device con-

ductance in the linear bias regime without any adjustable parameters. Here we consider only weak ($\lesssim 0.1 T$) magnetic fields in order to study the effects of breaking time-reversal symmetry. We will present results for the edge state regime in a subsequent publication⁵.

We include donor layer disorder in the calculation and present results for the statistics of level spacings and partial level widths due to tunneling to the leads. Recently we have employed Monte-Carlo variable range hopping simulations to consider the effect of Coulomb regulated ordering of ions in the donor layer on the mode characteristics of split-gate quantum *wires*⁶. The results of those simulations are here applied to quantum dot electronic structure.

A major innovation in this calculation is our method for determining the two dimensional electron gas (2DEG) charge density. At each iteration of the self-consistent calculation, at each point in the $x-y$ plane we determine the subbands $\epsilon_n(x, y)$ and wave functions $\xi_n^{xy}(z)$ in the z (growth) direction. The full three dimensional density is then determined by a solution of the multi-component 2D Schrödinger equation and/or 2D Thomas-Fermi approximation.

Among the many approximation in the calculation are the following. We use the local density approximation (LDA) for exchange-correlation (XC), specifically the parameterized form of Stern and Das Sarma⁷. While the LDA is difficult to justify in small ($N \sim 50 - 100$) quantum dots it is empirically known to give good results in atomic and molecular systems where the density

is also changing appreciably on the scale of the Fermi wavelength⁸.

In reducing the 3D Schrödinger equation to a multi-component 2D equation we cutoff the expansion in subbands, often taking only the lowest subband into account. We also cutoff the wavefunctions by placing another artificial *AlGaAs* interface at a certain depth (typically 200 \AA) away from the first interface, thereby ensuring the existence of subbands at all points in the $x-y$ plane. Generally the subband energy of this bare square well is much smaller than the triangular binding to the interface in all but those regions which are very nearly depleted.

The dot electron states in the zero magnetic field regime are simply treated as spin degenerate. For $B \neq 0$ an unrenormalized Landé g -factor of -0.44 is used. We employ the effective mass approximation uncritically and ignore the effective mass difference between *GaAs* and *AlGaAs* ($m^* = 0.067 m_0$). Similarly we take the background dielectric constant to be that of pure *GaAs* ($\kappa = 12.5$) thereby ignoring image effects (in the *AlGaAs*). We ignore interface grading and treat the interface as a sharp potential step. These effects have been treated in other calculations of self-consistent electronic structure for *GaAs* – *AlGaAs* devices⁷ and have generally been found to be small.

We mostly employ effective atomic units wherein $1 \text{ Ry}^* = m^* e^4 / 2 \hbar^2 \kappa^2 \approx 5.8 \text{ meV}$ and $1 a_B^* = \hbar^2 \kappa / m^* e^2 \approx 100 \text{ \AA}$.

The structure of the paper is as follows. In section II we first discuss the calculation of the electronic structure, focusing on those features which are new to our method. Further subsections then consider the treatment of discrete ion charge and disorder, calculation of the total dot free energy from the self-consistent electronic structure results, calculation of the source-dot-drain conductance in the linear regime and calculation of the dot capacitance matrix. Section III provides new results which are further subdivided into basic electrostatic properties, properties of the effective single electron spectra, statistics of level spacings and widths and conductance in the Coulomb oscillation regime. Section IV summarizes the principal conclusions which we derive from the calculations.

II. CALCULATIONS

A. Quantum dot self-consistent electronic structure

We consider a lateral quantum dot patterned on a 2DEG heterojunction via metallic surface gates (Fig. 1). At a semiclassical level, other gate geometries, such as a simple point contact or a multiple dot system, can be treated with the same method^{6,9}. However, a full 3D solution of Schrödinger's equation, even employing our subband

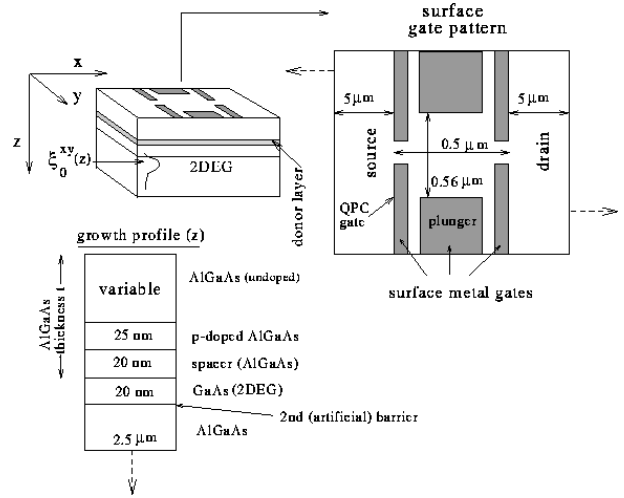


FIG. 1. Schematic of device used in calculation. The z -subband structure throughout the plane are calculated at each iteration of the self-consistency loop. Most results presented with gate variation assume that both the upper and lower pins of the relevant gate are simultaneously varied.

expansion procedure for the z direction, is only tractable in the current method when a region with a small number of electrons ($N \leq 100$) is quantum mechanically isolated, such as in a quantum dot.

1. Poisson equation and Newton's method

In principal, a self-consistent solution is obtained by iterating the solution of Poisson's equation and *some* method for calculating the charge density (see following sections II.A.2 and II.A.3). In practise, we follow Kumar *et al*¹⁰ and use an \mathcal{N} -dimensional Newton's method for finding the zeroes of the functional $\vec{F}(\vec{\phi}) \equiv \Delta \cdot \vec{\phi} + \vec{\rho}(\vec{\phi}) + \vec{q}$; where the potential, ϕ_i , and density, ρ_i , on the \mathcal{N} discrete lattice sites ($\mathcal{N} \sim 100,000$) are written as vectors, $\vec{\phi}$ and $\vec{\rho}$. The vector \vec{q} represents the inhomogeneous contribution from any Dirichlet boundary conditions, Δ is the Laplacian (note that here it is a matrix, not a differential operator), modified for boundary conditions. Innovations for treating the Jacobian $\partial \rho_i / \partial \phi_j$ beyond 3D Thomas-Fermi, and for rapidly evaluating the mixing parameter t (see Ref.¹⁰) are discussed below.

The Poisson grid spans a rectangular solid and hence the boundary conditions on six surfaces must be supplied. Wide regions of the source and drain must be included in order to apply Neumann boundary conditions on these ($x = \text{constant}$) interfaces, so a non-uniform mesh is essential. It is also possible to apply Dirichlet boundary conditions on these interfaces using the ungated wafer (one dimensional) potential profile calculated off-line¹¹. In this case, failure to include sufficiently wide lead regions shows up as induced charge on these surfaces (non-vanishing electric field). To keep the total induced charge on all surfaces below 0.5 electron, lead regions of

$\sim 5 \mu\text{m}$ are necessary, assuming a surface gate to 2DEG distance (i.e. AlGaAs thickness) of 1000 \AA . In other words we need an aspect ratio of $50 : 1$. We note that we ignore background compensation and merely assume that the Fermi level is pinned at some fixed depth (“ z_∞ ” $\sim 2.5 \mu\text{m}$) into the GaAs at the donor level. The donor energy for GaAs is taken as 1 Ry^* below the conduction band. In the source and drain regions, the potential of the 2DEG Fermi surface is fixed by the desired (input) lead voltage.

We apply Neumann boundary conditions at the $y = \text{constant}$ surfaces. The $z = 0$ surface of the device has Dirichlet conditions on the gated regions (voltage equal to the relevant desired gate voltage) and Neumann conditions, $\partial\phi/\partial n = 0$, elsewhere. This is equivalent to the “frozen surface” approximation of¹², further assuming a high dielectric constant for the semiconductor relative to air. Further discussion of this semiconductor-air boundary condition can be found in Ref.¹².

2. Charge density, quasi-2D treatment

The charge density *within* the Poisson grid (i.e. not surface gate charge) includes the 2DEG electrons and the ions in the donor layer. The treatment of discreteness, order and disorder in the donor ionic charge \vec{p}_{ion} has been discussed in Ref.⁶ in regards to quantum wire electronic structure. Some further relevant remarks are made below in section II.B.

As noted above, we take advantage of the quasi-2D nature of the electrons at the $\text{GaAs} - \text{AlGaAs}$ interface to simplify the calculation for their contribution to the total charge. Given $\vec{\phi}$, we begin by solving Schrödinger’s Eq. in the z -direction *at every point* in the $x - y$ plane,

$$\left[-\frac{\partial^2}{\partial z^2} + V_B(z) + e\phi(x, y, z)\right]\xi_n^{xy}(z) = \epsilon_n(x, y)\xi_n^{xy}(z) \quad (1)$$

where $V_B(z)$ is the potential due to the conduction band offset between GaAs and $\text{Al}_x\text{Ga}_{1-x}\text{As}$. We generally employ fast Fourier transform with 16 or 32 subbands.

In order that there be a discrete spectrum at each point in the $x - y$ plane, it is convenient to take $V_B(z)$ as a *square well* potential (Fig. 1). That is, we effectively cutoff the wave function with a second barrier, typically 200 \AA from the primary interface. In undepleted regions the potential is still basically triangular and only the tail of the wave function is affected. However, near the border between depleted and undepleted regions the artificial second barrier will introduce some error into the electron density. This is because as a depletion region is approached, the binding *electric field* at the 2DEG interface (slope of the triangular potential) reduces, in addition to the interface potential itself rising. Consequently, all subbands become degenerate and *near the edge electrons are three dimensional*¹⁴. We have checked that this

departure from interface confinement, and in general in-plane gradients of $\xi_n^{x,y}(z)$ contribute negligibly to quantum dot level energies. However, theoretical descriptions of 2DEG edges commonly assume perfect confinement of electrons in a plane. In particular the description of edge excitations in the quantum Hall effect regime in terms of a chiral Luttinger liquid¹⁵ may be complicated in real samples by the emergence of this vanishing energy scale and collective modes related to it.

Assuming only a single z -subband now and dropping the index n , we determine the charge distribution in the $x - y$ plane from the effective potential $\epsilon(x, y)$, employing a 2D Thomas-Fermi approximation for the charge in the leads and solving a 2D Schrödinger equation in the dot. In order that the dot states be well defined, the QPC saddle points must be classically inaccessible. (If this is not the case it is still possible to use a Thomas-Fermi approximation throughout the plane for the charge density^{6,9}). In the dot, the density is determined from the eigenstates by filling states according to a Fermi distribution either to a prescribed “quasi-Fermi energy” of the dot, or to a fixed number of electrons. It has been pointed out that a Fermi distribution for the level occupancies in the dot is an inaccurate approximation to the correct grand canonical ensemble distribution³. Nonetheless, for small dots ($N \lesssim 15$) Jovanovic *et al.*¹⁶ have shown that, regarding the filling factor, the discrepancy between a Fermi function evaluation and that of the full grand canonical ensemble is $\sim 5\%$ at half filling and significantly smaller away from the Fermi surface. As N increases the discrepancy should become smaller.

3. Solution of Schrödinger’s equation in the dot

To solve the effective 2D Schrödinger’s equation in the dot,

$$(-\nabla^2 + \epsilon(\mathbf{x}))f(\mathbf{x}) = Ef(\mathbf{x}) \quad (2)$$

we set the 2D potentials throughout the *leads* to their values at the saddle points, thereby ensuring that the wave functions decay uniformly into the leads. Thus the energy of the higher lying states will be shifted upward slightly. In seeking a basis in which to expand the solution of Eq. 2 we must consider the approximate shape of the potential. The quantum dots which we model here are lithographically approximately square in shape. However the potential at the 2DEG level and also the effective 2-D potential $\epsilon(r, \theta)$, (now in polar coordinates) are to lowest order azimuthally symmetric. The *radial* dependence of the potential is weakly parabolic across the center. Near the perimeter higher order terms become important (cf. figure 2b and Eq. 15).

As the choice of a good basis is not completely clear, we have tried two different sets of functions: Bessel functions and the so-called Darwin-Fock (DF) states¹⁷. The

details of the solution for the eigenfunctions and eigenvalues differ significantly whether we use the Bessel functions or the DF states. The Bessel function case is largely numerical whereas the DF functions together with polynomial fitting of the azimuthally symmetric part of the radial potential allow a considerable amount of the work to be done analytically. Further, neither of the two bases comes particularly close to fitting the somewhat eccentric shape of the actual dot potential. It is therefore gratifying that comparing the eigenvalues determined from the two bases when reasonable cutoffs are used, we find for up to the 50th eigenenergy agreement to three significant figures, or to within roughly 5 *micro eV*.

4. Summary and efficiency

To summarize the calculation, we begin by choosing the device dimensions such as the gate pattern, the ionized donor charge density and its location relative to the 2DEG, the aluminum concentration for the height of the barrier, and the thickness of the *AlGaAs* layer. We construct non-uniform grids in x , y and z that best fit the device within a total of about 10^5 points. Gate voltages, temperature, source-drain voltages, and either the electron number N or the quasi-Fermi energy of the dot are inputs. The iteration scheme begins with a guess of $\vec{\phi}^{(0)}$. The 1-D Schrödinger equation is solved at each point in the $x - y$ plane and an effective 2-D potential $\epsilon(x, y)$ for one or at most two subbands is thereby determined. Taking $|\xi_n^{xy}(z)|^2$ for the z -dependence of the charge density, we compute the 2D dependence in the leads using a 2D Thomas-Fermi approximation and in the dot by solving Schrödinger's equation and filling the computed states according to a Fermi distribution. We compute $\vec{F}(\vec{\phi}^{(0)})$, which is a measure of how far we are from self-consistency, and solve for $\delta\vec{\phi}$, the potential increment, using a mixing parameter t . This gives the next estimate for the potential $\vec{\phi}^{(1)}$. The procedure is iterated and convergence is gauged by the norm of F .

In practise there are many tricks which one uses to hasten (or even obtain !) convergence. First, we use a scheme developed by Bank and Rose^{18,10} to search for an optimal mixing parameter t . Repeated calculation of Schrödinger's equation, which is very costly, is in principle required in the search for t . Far from convergence the Thomas-Fermi approximation can be used in the dot as well as the leads. Nearer to convergence we find that diagonalizing $t \delta\vec{\phi}$ in a basis of about ten states near the Fermi surface, treating the charge in the other filled states as inert, is highly efficient. Periodically the full solution of Schrödinger's equation is employed to update the wave functions.

The wave function information is also used to make a better estimate of $\partial\rho_i/\partial\phi_i$. The 3D Thomas-Fermi method for estimating this quantity does not account for the fact that the change in density at a given grid point

will be most strongly influenced by the changes in the occupancies of the partially filled states at the Fermi surface. Thus use of these wave functions greatly improves the speed of the calculation.

B. Disorder

Evidence of Coulombic *ordering* of the donor charge in a modulation doping layer adjacent to a 2DEG has recently accumulated¹⁹. When the fraction \mathcal{F} of ionized donors among all donors is less than unity, redistribution of the ionized sites through hopping can lead to ordering of the donor layer charge^{20,6}.

In this paper we consider the effects of donor charge distribution on the statistical properties of quantum dot level spectra, in particular the unfolded level spacings, and on the connection coefficients to the leads Γ_p of the individual states (see below). These dot properties are calculated with ensembles of donor charge which range from completely random (identical to $\mathcal{F} = 1$, no ion re-ordering possible) to highly ordered ($\mathcal{F} \sim 1/10$). For a discussion of the glass-like properties of the donor layer and the Monte-Carlo variable range hopping calculation which is used to generate ordered ion ensembles, see Refs.⁶ and²¹.

Note that hopping is assumed to take place at temperatures (~ 160 K) much higher than the sub-liquid Helium temperatures at which the dot electronic structure is calculated. Thus the ionic charge distributions generated in the Monte-Carlo calculation are, for the purposes of the 2DEG electronic structure calculation, considered fixed space charges which are specifically not treated as being in thermal equilibrium with the 2DEG.

The region where the donor charge can be taken as discrete is limited by grid spacing and hence computation time. In the wide lead regions and wide region lateral to the dot the donor charge is always treated as "jellium." Also, to serve as a baseline, we calculate the dot structure with jellium across the dot region as well. We introduce the term "quiet dot" to denote this case.

C. Free energy

To calculate the total interacting free energy we begin from the semi-classical expression

$$F(\{n_p\}, Q_i, V_i) = \sum_p n_p \epsilon_p^0 + \frac{1}{2} \sum_i^M Q_i V_i - \sum_{i \neq \text{dot}} \int dt V_i(t) I_i(t) \quad (3)$$

where n_p are the occupancies of non-interacting dot energy levels ϵ_p^0 ; Q_i and V_i are the charges and voltages of the M distinct "elements" into which we divide the system: dot, leads and gates. I_i are the currents supplied by power supplies to the elements.

The *self-consistent* energy levels for the electrons in the dot are $\epsilon_p = \langle \psi_p | -\nabla^2 + V_B(z) + e\phi(\mathbf{r}) | \psi_p \rangle$. A

sum over these levels double counts the electron-electron interaction. Thus, for the terms in Eq. 3 relating to the dot, we make the replacement:

$$\sum_p n_p \varepsilon_p^0 + \frac{1}{2} Q_{dot} V_{dot} \rightarrow \sum_p n_p \varepsilon_p - \frac{1}{2} \int d\mathbf{r} \rho_{dot}(\mathbf{r}) \phi(\mathbf{r}) + \frac{1}{2} \int d\mathbf{r} \rho_{ion}(\mathbf{r}) \phi(\mathbf{r}) \quad (4)$$

where $\rho_{dot}(\mathbf{r})$ refers only to the charge in the dot states and $\rho_{ion}(\mathbf{r})$ refers to all the charge in the donor layer.

We have demonstrated^{28,22} that previous investigations^{3,23} had failed to correctly include the work from the power supplies, particularly to the source and drain leads, in the energy balance for tunneling between leads and dot in the Coulomb blockade regime. Here, we assume a low impedance environment which allows us to make the replacement:

$$\frac{1}{2} \sum_{i \neq dot} Q_i V_i - \sum_{i \neq dot} \int dt V_i(t) I_i(t) \rightarrow -\frac{1}{2} \sum_{i \neq dot} Q_i V_i. \quad (5)$$

The charges on the gates are determined from the gradient of the potential at the various surface regions, the voltages being given. Including only the classical electrostatic energy of the leads, the total free energy is⁴:

$$F(\{n_p\}, N, V_i) = \sum_p n_p \varepsilon_p - \frac{1}{2} \int d\mathbf{r} \rho_{dot}(\mathbf{r}) \phi(\mathbf{r}) + \frac{1}{2} \int d\mathbf{r} \rho_{ion}(\mathbf{r}) \phi(\mathbf{r}) - \frac{1}{2} \sum_{i \in leads} \int d\mathbf{r} \rho_i(\mathbf{r}) \phi(\mathbf{r}) - \frac{1}{2} \sum_{i \in gates} Q_i V_i \quad (6)$$

where the energy levels, density, potential and induced charges are implicitly functions of N and the applied gate voltages V_i . Note that the occupation number dependence of these terms is ignored. In the $T = 0$ limit the electrons occupy the lowest N states of the dot, and the free energy is denoted $F_0(N, V_i)$.

D. Conductance

The master equation formula for the linear source-drain conductance through the dot, derived by several authors^{3,2,24} for the case of a fixed dot spectrum, is modified to the self-consistently determined free energy case as follows⁴:

$$G(V_g) = \frac{e^2}{k_B T} \sum_{\{n_i\}} P_{eq}(\{n_i\}) \sum_p \delta_{n_p,0} \frac{\Gamma_p^s \Gamma_p^d}{\Gamma_p^s + \Gamma_p^d} \times f(F(\{n_i + p\}, N + 1, V_g) - F(\{n_i\}, N, V_g) - \mu) \quad (7)$$

where the first sum is over dot level occupation configurations and the second is over dot levels. The equilibrium probability distribution $P_{eq}(\{n_i\})$ is given by the Gibbs distribution,

$$P_{eq}(\{n_i\}) = \frac{1}{Z} \exp[-\beta(F(\{n_i\}, N, V_g) - \mu)] \quad (8)$$

and the partition function is

$$Z \equiv \sum_{\{n_i\}} \exp[-\beta(F(\{n_i\}, N, V_g) - \mu)] \quad (9)$$

note that the sum on occupation configurations, $\{n_i\}$, includes implicitly a sum on N . In Eq. 7 f is the Fermi function, μ is the electrochemical potential of the source and drain and $\Gamma_p^{s(d)}$ are the elastic couplings of level p to source (drain). The notation $\{n_i + p\}$ denotes the set of occupancies $\{n_i\}$ with the p^{th} level, previously empty by assumption, filled. In Eq. 7 it is assumed that only a single gate voltage, V_g (the “plunger gate”, cf. Fig. 1), is varied.

E. Tunneling coefficients

The elastic couplings in Eq. 7 are calculated from the self-consistent wave functions²⁵:

$$\hbar \Gamma_{np} = 4\kappa^2 W_n^2(a, b) \left| \int dy f_p(x_b, y) \chi_n^*(x_b, y) \right|^2 \quad (10)$$

where $f_p(x_b, y)$ is the two dimensional part of the p^{th} wave function evaluated at the midpoint of the barrier, x_b , and $\chi_n^*(x_b, y)$ is the n^{th} channel wavefunction decaying into the barrier from the leads, $W_n(a, b)$ is the barrier penetration factor between the classical turning point in the lead and the point x_b , for channel n computed in the WKB approximation, and κ is the wave vector at the matching point. Though the channels are 1D we use the two dimensional density of states characteristic of the wide 2DEG region²⁶.

F. Capacitance

Quantum dot system electrostatic energies are commonly estimated on the basis of a capacitance model²⁷. When the self-consistent level energies and potential are known the total free energy can be computed without reference to capacitances. However, the widespread use of this model and the ease with which capacitances can be calculated from our self-consistent results (see below) encourages a discussion.

For a collection of N metal elements with charges Q_i and voltages V_j the capacitance matrix, defined by^{28,29} $Q_i = \sum_{j=1}^N C_{ij} V_j$, can be written in terms of the Green's function $G_D(\mathbf{x}, \mathbf{x}')$ for Laplace's equation satisfying Dirichlet boundary conditions on the element surfaces:

$$C_{ij} = \frac{1}{4\pi^2} \int d\Omega_i \int d\Omega_j \hat{n}_j \cdot \vec{\nabla}_x(\hat{n}_i \cdot \vec{\nabla}_{x'} G_D(\mathbf{x}, \mathbf{x}')) \quad (11)$$

where the integrals are over element surfaces with \hat{n}_j the outward directed normal.

In a system with an element of size L not much greater than the screening length λ_s , the voltage of the component, and hence the capacitance, is not well defined^{29,30}. In this case, as discussed in reference²⁹, the capacitance can no longer be written in terms of the solution of Poisson's equation alone, but must take account of the full self-consistent determination of the i^{th} charge distribution $\rho_i(\mathbf{x})$ from the j^{th} potential $\phi_j(\mathbf{x}) \forall i, j$. In general the capacitance will then become a kernel in an integral relation. A relationship of this kind has recently been derived in terms of the Linhard screening function by Büttiker³⁰.

To compute the dot self-capacitance from the calculated self-consistent electronic structure we have three separate procedures. In all three cases we vary the Fermi energy of the dot by some small amount to change the net charge in the dot. This requires that the QPCs be closed. For the first method the total charge variation of the dot is divided by the change in the electrostatic potential minimum of the dot. This is taken as the dot self-capacitance C_{dd} . A second procedure for the dot self-capacitance is to divide the change in the dot charge simply by the fixed, imposed change of the Fermi energy. This result is denoted C'_{dd} . Since the change in the potential minimum of the dot is not always equal to the change of the Fermi energy these results are not identical. Finally, we can fit the computed free energy $F(N, V_g)$ to a parabola in N at each V_g . If the quadratic term is αN^2 then the final form for the self-capacitance is $C''_{dd} = 1/(2\alpha)$ (primes are *not* derivatives here). This form, which also serves as a consistency check on our functional for the energy, is generally quite close to the first form and we present no results for it.

For the capacitances between dot and gates or leads, the extra dot charge (produced by increasing the Fermi energy in the dot) is screened in the gates and the leads so that the net charge inside the system (including that on the gated boundaries) remains zero. The fraction of the charge screened in a particular element gives that element's capacitance to the dot as a fraction of C_{dd} .

III. RESULTS

We consider only a small subspace of the huge available parameter space. For the results presented here we have fixed the nominal 2DEG density to $1.4 \times 10^{11} \text{ cm}^{-2}$ and the aluminum concentration of the barrier to 0.3. The lithographic gate pattern is shown in figure 1, as is the growth profile (including our artificial second barrier). Some results are presented with a variation of the total thickness t of the AlGaAs (Fig. 1).

To interpret the results we note the following considerations. Hohenberg-Kohn-Sham theory provides only that the ground state energy of an interacting electron system can be written as a functional of the density^{31,32}. The single particle eigenvalues ε_p have, strictly speaking, no

physical meaning. However, as pointed out by Slater⁸, the usefulness of DF theory depends to some extent on being able to interpret the energies and wave functions as some kind of single particle spectrum. In the Coulomb blockade regime it is particularly important to be clear what that interpretation, and its limitations, are.

A distinction is commonly made between the addition spectrum and the excitation spectrum for quantum dots^{33,34}. Differences between our effective single particle eigenvalues represent an approximation to the excitation spectrum. As a specific example, in the absence of depolarization and excitonic effects the first single particle excitation from the N -electron ground state with gate voltages V_i is $\varepsilon_{N+1}(N, V_i) - \varepsilon_N(N, V_i)$.

The addition spectrum, on the other hand, depends on the energy difference between the ground states of the dot *interacting with its environment* at two different N . Thus, in our formalism, the addition spectrum is given by differences in $F(\{n_p\}, N, V_i)$ at neighboring N , possibly further modulated by excitations, i.e. differences in the occupation numbers $\{n_p\}$.

In contrast to experiment, the electronic structure can be determined for arbitrary N and V_i (so long as the dot is closed). This includes both non-integer N as well as values which are far from equilibrium (differing chemical potential) with the leads. The "resonance curve"⁴ is given by the N which minimizes $F_0(N, V_g)$ at each V_g (gates other than the plunger gate are assumed fixed). This occurs when the chemical potential of the dot equals those of the leads (which are taken as equal to one another and represent the energy zero) and gives the most probable electron number. Results presented below as a function of varying gate voltage, particularly the spectra in Figs. 9 and 13, are assumed to be along the resonance curve.

A. Electrostatics

Figure 2a shows an example of a potential profile along with a corresponding density plot for a quiet dot containing 62 electrons. The basic potential/density configuration, as well as the capacitances are highly robust. These data are computed completely in the 2D Thomas-Fermi approximation, single z -subband, at $T = 0.1 \text{ K}$. Solution of Schrödinger's equation or variation of T result in only subtle changes. The depletion region spreading is roughly 100 nm . Figure 2b shows a set of potential and density profiles along the y -direction (transverse to the current direction) in steps of $3.3 a_B^*$ in x , from the QPC saddle point to the dot center. Note that the density at the dot center is only about 65% of the ungated 2DEG

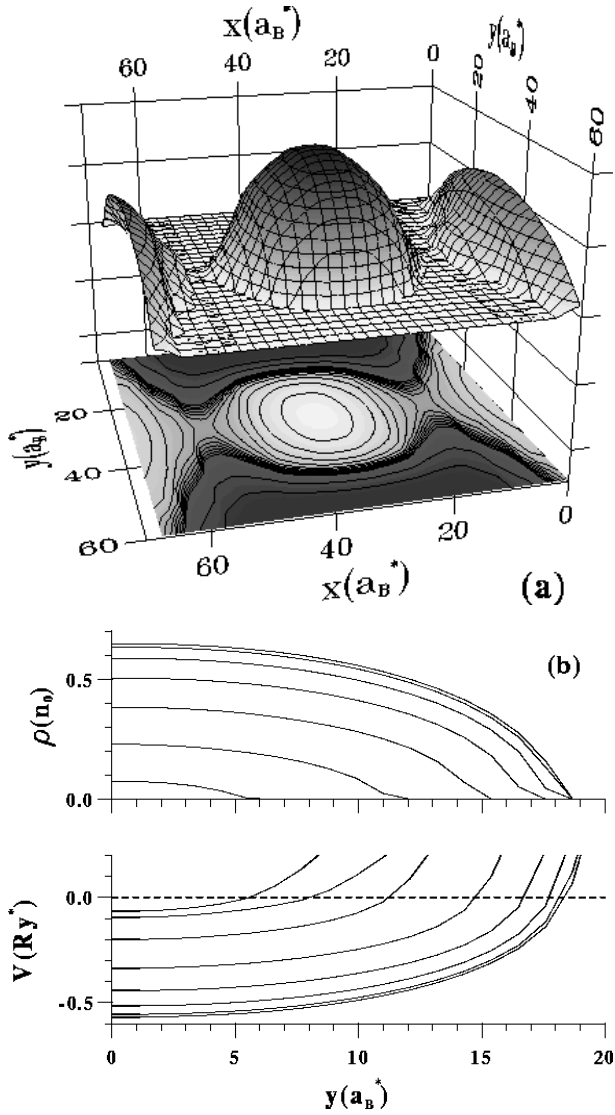


FIG. 2. (a) Contour plot for density and potential, quiet dot, TF. Isolines in potential spaced at $\sim 0.1 Ry^*$ up to $0.5 Ry^*$ above Fermi level, after which much more widely. Density isoline spacing $\sim 0.01 a_B^{*-2}$, maximum density $\sim 0.1 a_B^{*-2}$. Ripples near QPCs are finite grid size effect; plotted $x-y$ mesh shows every other grid line. (b) Transverse (y -direction) half-profiles of density and potential corresponding to (a), taken at $3.3 a_B^*$ intervals from dot center. Uppermost potential trace, entirely above Fermi surface, is in QPC ($x \approx 54 a_B^*$ in Fig. 2a) where density is zero. Density is scaled to nominal 2DEG value $0.14 a_B^{*-2} \approx 1.4 \times 10^{11} cm^{-2}$.

density. Correspondingly the potential at the center is above the floor of the ungated 2DEG ($\sim -0.9 Ry^*$).

We discuss a simple model for the potential shape of a circular quantum dot below (Sec. III.B.1). Here we note only that the radial potential can be regarded as parabolic to lowest order with quartic and higher order corrections whose influence increases near the perimeter. In Thomas-Fermi studies on larger dots^{22,9} with a comparable aspect ratio we find that the potential and density

achieve only 90 % of their ungated 2DEG value nearly $200 nm$ from the gate. Regarding classical billiard calculations for gated structures therefore^{35–38} even in the absence of impurities it is difficult to see how the “classical” Hamiltonian at the 2DEG level can be even approximately integrable unless the lithographic gate pattern is azimuthally symmetric³⁹.

The importance of the remote ionized impurity distribution is demonstrated in figure 3 which shows a quantum dot with randomly placed ionized

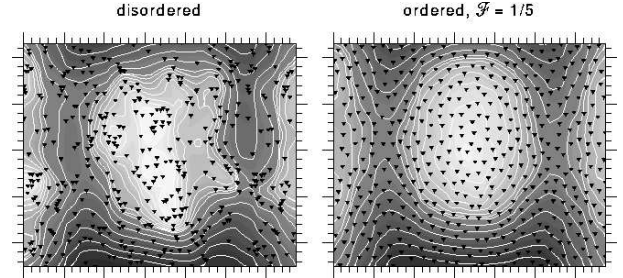


FIG. 3. Contour plots of dot showing ion placement for disordered case (left) and ordered ($\mathcal{F} = 1/5$) ion distribution, TF. Isolines at $0.08 Ry^*$ up to Fermi surface, wider thereafter. Gate voltages and locations identical in the two cases. Note particularly position of right QPC determined by ions in disordered case.

donors on the left and with ions which have been allowed to reach quasi-equilibrium via variable range hopping, on the right. In both cases the total ion number in the area of the dot is fixed. The example shown here for the ordered case assumes, in the variable range hopping calculation, one ion for every five donors ($\mathcal{F} = 1/5$). As in Ref.⁶ we have, for simplicity, ignored the negative U model for the donor impurities (DX centers), which is still controversial^{19,40,41}. If the negative U model, at some barrier aluminum concentration, is correct, the most ordered ion distributions will occur for $\mathcal{F} = 1/2$, as opposed to the neutral DX picture employed here, where ordering increases monotonically as \mathcal{F} decreases⁴².

For these assumptions figure 4 indicates that ionic ordering substantially reduces the potential fluctuations relative to the completely disordered case, even for relatively large \mathcal{F} . Here, using ensembles of dots with varying \mathcal{F} we compare the effective 2D potential with a quiet dot (jellium donor layer) at the same gate voltages and same dot electron number. The distribution of the potential deviation is computed as:

$$P(\Delta V) = \frac{1}{SN^2} \sum_s \sum_{i,j} \delta(\Delta V - [V_{\mathcal{F}}(x_i, y_j) - V_{qd}(x_i, y_j)]) \quad (12)$$

where s labels samples (different ion distributions), typically up to $S = 10$, N is the total number of x or y grid points in the dot (~ 50), and “qd” stands for quiet dot. The distributions for all \mathcal{F} are asymmetric (Fig. 4). Although the means are indistinguishably close to zero, the

probability for large potential hills resulting from disorder is greater than for deep depressions. Also, the distributions for points above the Fermi surface (dashed lines) are broader by an order of magnitude (in standard deviation) than below, due to screening. Finally, saturation as $\mathcal{F} \rightarrow 0$ (inset Fig. 4) shows that even if the ions are arranged in a Wigner crystal (the limiting case at $\mathcal{F} = 0$), potential fluctuations would be expected in comparison with ionic jellium.

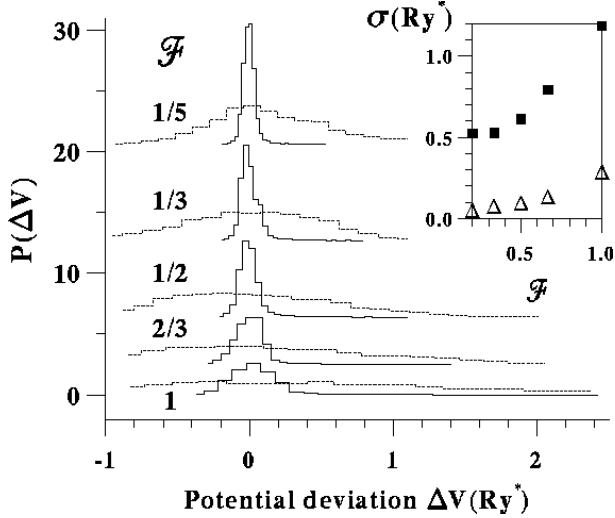


FIG. 4. Histograms of deviation of effective 2D potential from quiet dot values at the same x, y point and same gate voltages, for several ion to donor ratios \mathcal{F} , TF. Solid lines are statistics for points below Fermi surface, dashed lines, showing substantially more variation, above. $\mathcal{F} = 1$ is completely random (disordered) case. Distributions uniformly asymmetric, positive potential deviations from quiet dot case being more likely, but means are very close to zero. Inset shows standard deviation of histograms versus \mathcal{F} , triangle below, squares above Fermi level.

The success of the capacitance model in describing experimental results of charging phenomena in mesoscopic systems has been remarkable²⁷. For our calculations as well, even the simplest formulations for the capacitance tend to produce smoothly varying results when gate voltages or dot charge are varied. Figure 5 shows the trend of the dot self-capacitances with V_g . Also shown are the equilibrium dot electron number N and the minimum of the dot potential V_{min} as functions of V_g . Note here that V_{min} is the minimum of the 3D electrostatic potential rather than the effective 2D potential which is presented elsewhere (such as in Figs. 2 and 3).

That C_{dd} generally decreases as the dot becomes smaller is not surprising and has been discussed elsewhere⁴³. All three forms of C_{dd} are roughly in agreement giving a value ~ 2 fF (the capacitance as calculated from the free energy is not shown). The fluctuations result from variations in the quantized level energies as the dot size and shape are changed by V_g . Note that *numerical* error is indiscernible on the scale of the fig-

ure. The pronounced collapse of C'_{dd} near $V_g = -1.15$ V, which is expanded in the upper panel, shows the presence of a region where the change of N with E_F is greatly suppressed. Since the change of V_{min} with E_F is similarly suppressed there is no corresponding anomaly in C_{dd} . Interestingly, the capacitance computed from the free energy also reveals no deep anomaly.

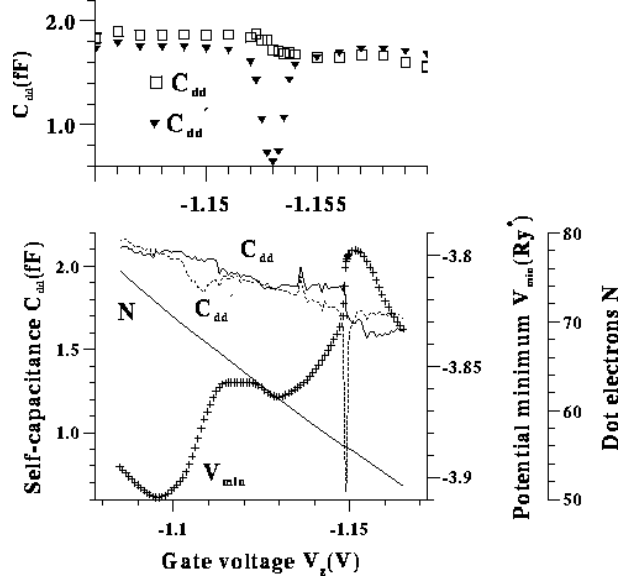


FIG. 5. Dot self-capacitances, equilibrium electron number and potential minimum as a function of plunger gate voltage (lower). *Numerical* uncertainty is indiscernible, so variations of C_{dd} are real and related to spectrum. C'_{dd} calculated using ΔE_F rather than ΔV_{min} , so strong anomaly near -1.15 V due to rigidity of N . Upper panel: expanded view of capacitances near anomaly; cf. spectrum, Fig. 9.

The anomaly at $V_g = -1.15$ V and also the fluctuation in the electrostatic properties near -1.1 V are related to a shell structure in the spectrum which we discuss below.

A frequently encountered model for the classical charge distribution in a quantum dot is the circular conducting disk with a parabolic confining potential^{44,45}. It can be shown (solving, for example, Poisson's equation in oblate spheroidal coordinates) that for such a model the 2D charge distribution in the dot goes as

$$n(r) = n(0)(1 - r^2/R^2)^{1/2} \quad (13)$$

where R is the dot radius and $n(0) = 3N/2\pi R^2$ is the density at the dot center. The “external” confining potential is assumed to go as $V(r) = V_0 + kr^2/2$ and R is related to N through

$$R = \frac{3\pi}{4} \frac{e^2}{\kappa k} N \quad (14)$$

where κ is the dielectric constant⁴⁴.

To justify this model, the authors of Ref.⁴⁴ claim that the calculations of Kumar *et al.*¹⁰ show that “the confinement...has a nearly parabolic form for the external

confining potential (*sic*).” This is incorrect. What Kumar *et al.*’s calculations shows is that (for $N \lesssim 12$) the *self-consistent* potential, which includes the potential from the electrons themselves, is approximately cut-off parabolic. The *external* confining potential, as it is used in Ref.⁴⁴, would be that produced by the donor layer charge and the charge on the surface gates only. We introduce a simple model (see III.B.1 below) wherein this confining potential charge is replaced by a circular disk of positive charge whose density is fixed by the doping density and whose radius is determined by the number of electrons *in the dot*. The gates can be thought of as merely cancelling the donor charge outside that radius. The essential point, then, is this: adding electrons to the dot decreases the (negative) charge on the gates and therefore increases the radius. One can make the assumption, as in Ref.⁴⁴, that the external potential is parabolic, but it is a mistake to treat that parabolicity, k , as independent of N .

This is illustrated in figure 6 where we have plotted contours for the *change* in the 2D density, as E_F is incrementally increased,

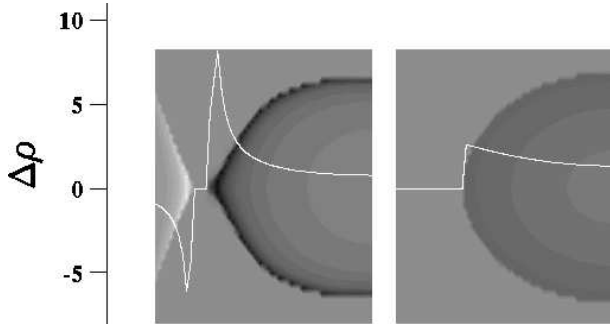


FIG. 6. Grey scale of density change as Fermi energy in dot is raised relative to leads, Thomas-Fermi (TF). Total change in N about 1.4 electrons. Screening charge, white region, in leads is positive. White curve gives profile along line bisecting dot, scaled to average change of N per unit area. Right panel shows model of Ref.⁴⁴ where confining potential has fixed parabolicity. Note that this model drastically underestimates degree to which charge is added to perimeter.

as determined self-consistently (Thomas-Fermi everywhere, left panel) and as determined from Eq. 13. The white curves display the density change profiles across the central axis of the dot. The total change in N is the same in both cases, but clearly the model of Eq. 13 underestimates the degree to which new charge is added mostly to the perimeter.

Recently the question of charging energy renormalization via tunneling as the conductance G_0 through a QPC approaches unity has received much attention^{46–48}. In a recent experiment employing two dots in series a splitting of the Coulomb oscillation peaks has been observed as the central QPC (between the two dots) is lowered⁴⁹. Perturbation theory for small G_0 and a model which treats

the decaying channel between the dots as a Luttinger liquid for $G_0 \rightarrow 1$ (e^2/h) lead to expressions for the peak splitting which is linear in G_0 in the former case and goes as $(1 - G_0)\ln(1 - G_0)$ in the latter case.

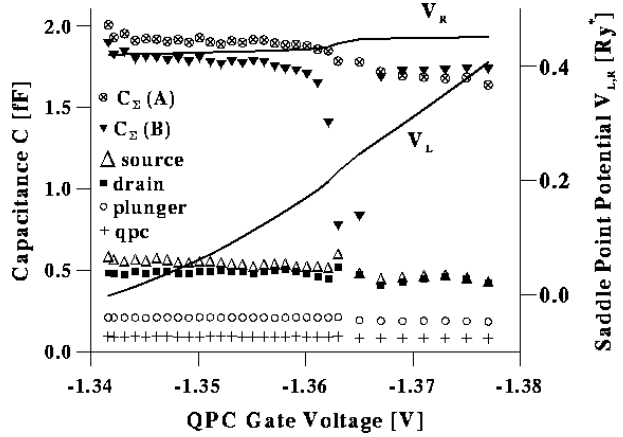


FIG. 7. Variation of dot capacitances with QPC voltage (gates 1 and 4 in figure 1). Solid lines for $V_{L(R)}$ are effective 2D potential for left (right) saddle point (right hand scale). $C_\Sigma(A)$ and $C_\Sigma(B)$ are dot self-capacitances (cf. Fig. 5) computed using ΔV_{min} and ΔE_F respectively. “Source” is (arbitrarily) outside *left* saddle point. Note that V_L goes practically to zero but the dot capacitance to the source only marginally increases relative to dot to drain capacitance. Capacitances for QPC and plunger are for a single finger only in each case. Anomaly related to dot reconstruction also visible here as QPC voltage is changed.

A crucial assumption of the model, however, is that the “bare” capacitance, specifically that between the dots C_{d1-d2} , remains approximately independent of the height of the QPC, even when an open channel connects the two dots. Thus the mechanism of the peak splitting is assumed to be qualitatively different from a model which predicts peak splitting entirely on an electrostatic basis when the inter-dot capacitance increases greatly⁵⁰. The independence of C_{d1-d2} from the QPC potential is plausible insofar as most electrons, even when a channel is open, are below the QPC saddle points and hence localized on either one dot or the other. Further, if the screening length is short and if the channel itself does not accommodate a significant fraction of the electrons, there is little ambiguity in retaining C_{d1-d2} to describe the gross electrostatic interaction of the dots, even when the dots are *connected* at the Fermi level.

In figure 7 we present evidence for this theory by showing the capacitance between a dot and the *leads* as the QPC voltage is reduced. In the figure $V_{L(R)}$ is the effective 2D potential of the left (right) saddle point as the left QPC gate voltages V_{QPC} only are varied. The dot is nearly open when the QPC voltages (both pins on the left) reach ~ -1.34 V. The results here use the full quantum mechanical solution (without the LDA exchange-correlation energy), however the electrons in the lead

continue to be treated with a 2D TF approximation. The dot “reconstruction” seen in figure 4 is visible

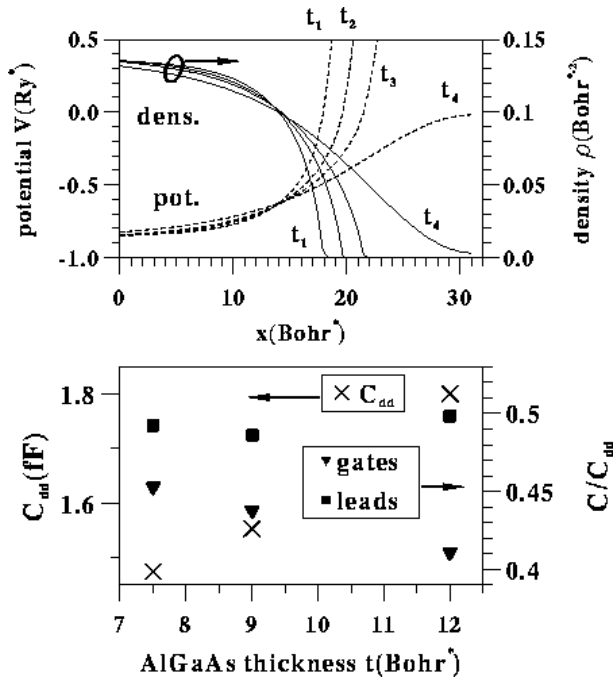


FIG. 8. *AlGaAs* thickness dependence of capacitances (lower). Self-capacitance decreases as gates get closer to 2DEG. Upper panel shows that, for smaller t the potential confinement is steeper and charge more compact, hence smaller C_{dd} . $t_1 = 5.25$, $t_2 = 7.5$, $t_3 = 9$, and $t_4 = 12 a_B^*$. Relative capacitance from dot to gates and leads fairly insensitive to t .

here also around $V_{QPC} = -1.365$ V. Note that the right saddle point is sympathetically affected when we change this left QPC. While the effect is faint, $\sim 5\%$ of the change of the left saddle, the sensitivity of tunneling to saddle point voltage (see also below) has resulted in this kind of cross-talk being problematical for experimentalists. The figure also shows that the capacitance between the dot and one lead exceeds that to a (single) QPC gate or even to a plunger gate. However the most important result of the figure is to show that the dot to lead capacitance is largely insensitive to QPC voltage. When the left QPC is as closed as the right ($V_{QPC} \sim -1.375$ V) the capacitances to the source and drain are equal. But even near the open condition the capacitance to the left lead (arbitrarily the “source”) only exceeds that to the drain (which is still closed) minutely. Therefore the assumptions of a “bare” capacitance which remains constant even as contact is made with a lead (or, in the experiment, another dot) seems to be very well founded.

As noted above, the interaction between a gate and the 2DEG depends upon the distance of the gates from the 2DEG, i.e., the *AlGaAs* thickness t . In figure 8 we show that, as we decrease t , simultaneously changing the gate

voltages such that N and the saddle point potentials remain constant, the total dot capacitance also decreases, but the distribution of the dot capacitance between leads, gates and (not shown) back gate change only moderately. That gates closer to the 2DEG plane should produce dots of lower capacitance is made clear in the upper panel of the figure, which shows the potential and density profile (using TF) near a depletion region at the side of the dot at varying t and constant gate voltage. For smaller t the depletion region is widened but the density achieves its ungated 2DEG value (here $0.14 a_B^{*-2}$) more quickly; a potential closer to hard walled is realized. In the presence of stronger confinement the capacitance decreases and the charging energy increases.

The profile of the tunnel barriers and the barrier penetration factors are also dependent on t . However we postpone a discussion of this until the section on tunneling coefficients.

B. Spectrum

The bulk electrostatic properties of a dot are, to first approximation, independent of whether a Thomas-Fermi approximation is used or Schrödinger’s equation is solved. A notable exception to this is the fluctuation in the capacitances. Figure 9 shows the plunger gate voltage dependence of the energy levels. The Fermi level of the dot is kept constant and equal to that of the leads (it is the energy zero). Hence as the gate voltage increases (becomes less negative) N increases.

Since the QPCs lie along the x -axis, the dot is never fully symmetric with respect to interchange of x and y , however the most symmetric configuration occurs for $V_g \sim -1.16$ V, towards the right side of the plot. The levels clearly group into quasi-shells with gaps between. The number of states per shell follows the degeneracy of a 2D parabolic potential, i.e. 1,2,3,4,... degenerate levels per shell (ignoring spin). There is a pronounced tendency for the levels to cluster at the Fermi surface, here given by $E = 0$, which we discuss below.

1. Shell structure

Shell structure in atoms arises from the approximate constancy of individual electron angular momenta, and degeneracy with respect to z -projection. Since in two dimensions the angular momentum m is fixed in the z (transverse) direction, the isotropy of space is broken and the only remaining manifest degeneracy, and this only for azimuthally symmetric dots, is with respect to $\pm z$. A two dimensional parabolic potential, in the absence of magnetic field, possesses an accidental degeneracy for which a shell structure is recovered.

We have shown above that modelling a quantum dot as a classical, conducting layer in an *external* parabolic

potential $kr^2/2$, where k is independent of the number of electrons in the dot, ignores the image charge in the surface gates forming the dot and therefore fails to properly describe the evolving charge distribution as electrons are added to the dot. A more realistic model, which *explains* the approximate parabolicity of the *self-consistent* potential, and hence the apparent shell structure, is illustrated in figure 10.

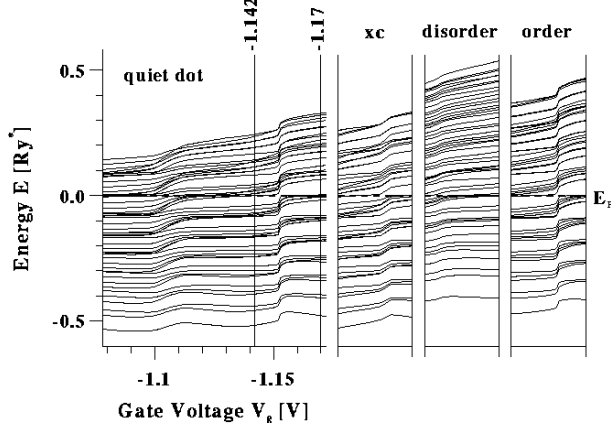


FIG. 9. Electronic spectrum showing level grouping into shells for quiet dot (Hartree), quiet dot with LDA exchange-correlation, disordered sample $\mathcal{F} = 1$ and ordered sample $\mathcal{F} = 1/5$. Range of gate voltage in latter three is from $V_g = -1.142$ to -1.17 V.

The basic electrostatic structure of a quantum dot, in the simplest approximation, can be represented by two circular disks, of radius R and homogeneous charge density σ_0 , separated by a distance a . The positive charge outside R is assumed to be cancelled by the surface gates. This approximation will be best for surface gates very close to the donor layer (i.e. small t). Larger *AlGaAs* thicknesses will require a non-abrupt termination

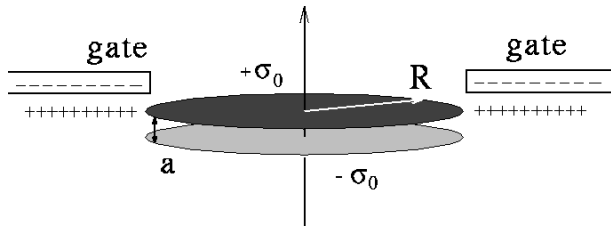


FIG. 10. Schematic for simple two charge disk model of quantum dot. Positive charge outside radius R taken to be uniformly cancelled by gates, electric charge in 2DEG mirrors positive charge. Resultant radial potential in 2DEG plane, Eq. 15, dominated by parabolic term inside R .

of the positive charge. In either case, the electronic charge is assumed in the classical limit to screen the background charge as nearly as possible. This is similar to the postulate in which wide parabolic quantum wells are expected to produce approximately homogeneous layers of electronic charge⁵¹.

A simple calculation for the radial potential (for $a < R$) in the electron layer ($z = 0$) gives, for the first few terms:

$$\phi(r) = \frac{2Ne}{\kappa R} [\sqrt{1 - a/R} - 1 + \frac{3}{8} \frac{a^2}{R^2} \frac{r^2}{R^2} - \frac{15}{32} \frac{a^4}{R^4} \frac{r^2}{R^2} + \frac{45}{128} \frac{a^2}{R^2} \frac{r^4}{R^4} + \dots] \quad (15)$$

where $Ne = \pi R^2 \sigma_0$ and κ is the background dielectric constant. While the coefficient of the quartic term is comparable to that of the parabolic term, the dependences are scaled by the dot radius R . Hence, the accidental degeneracy of the parabolic potential is broken only by coupling via the quartic term near the dot perimeter. This picture clearly agrees with the full self-consistent results wherein the parabolic degeneracy is observed for low lying states and a spreading of the previously degenerate states occurs nearer to the Fermi surface.

Comparison (not shown) of the potential computed from Eq. 15 and the radial potential profile (lowest curve, Fig. 2b) from the full self-consistent structure, shows good agreement for overall shape. However the former is about 25% smaller (same N) indicating that the sharp cutoff of the positive charge is, for these parameters, too extreme. However Eq. 15 improves for larger N and/or smaller t .

The wavefunction moduli squared associated with the Fig. 9 quiet dot levels for $V_g \sim -1.16$ V, $N \approx 54$ are shown schematically for levels 1 through 10 in figure 11, and for levels 11 through 35 in figure 12.

The lowest level in a shell is, for the higher shells, typically the most circularly symmetric. When the last member of a shell depopulates with V_g the inner shells expand outward, as can be seen near $V_g = -1.15$ V (Fig. 9) where level $p = 29$ depopulates. Since to begin filling a new shell requires the inward compression of the other shells and hence more energy, the capacitance decreases in a step when a shell is depopulated. The shell structure should have two distinct signatures in the standard (electrostatic) Coulomb oscillation experiment²⁷. First, since the self-capacitance drops appreciably (figure 5) when the last member of a shell depopulates, here N goes from 57 to 56, a concomitant discrete rise in the activation energy in the minimum between Coulomb oscillations can be predicted. Second, envelope modulation of peak heights⁴ occurs when excited dot states are thermally accessible as channels for transport, as opposed to the $T = 0$ case where the only channel is through the first open state above the Fermi surface (i.e. the $N + 1^{st}$ state). When N is in the middle of a shell of closely spaced, spin degenerate levels, the entropy of the dot, $k_B \ln \Omega$, where Ω is the number of states accessible to the dot, is sharply peaked. For example, for six electrons occupying six spin degenerate levels (i.e. twelve altogether)

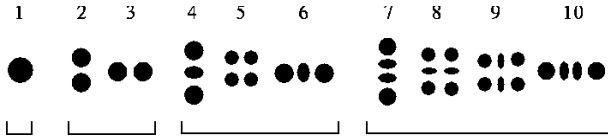


FIG. 11. Schematic showing the first ten levels of quiet dot. Shell structure consistent with $n+m = \text{constant}$, where n and m are nodes in x and y . Lower energy states show rectangular symmetry.

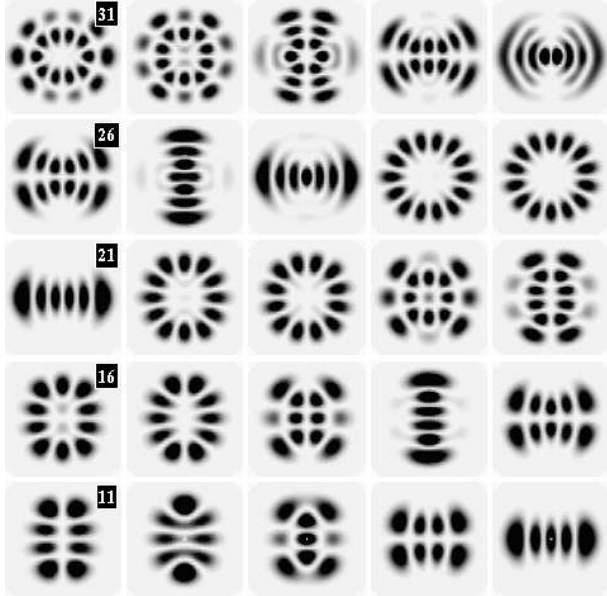


FIG. 12. Levels 11 through 35 (each spin degenerate) of quiet dot, Hartree. Circular symmetry increases with energy. States elongated in x (horizontal) most connected to leads.

all within $k_B T$ of the Fermi surface, the number of channels available for transport is 924. For eleven electrons in the shell, however, the number of channels reduces to 12. Consequently, minima and peaks of envelope modulation (see also figure 21 below) of CB oscillations which are frequently observed are clear evidence of level bunching, if not an organized shell structure.

Recently experimental evidence has accumulated for the existence of a shell structure as observed by inelastic light scattering⁵² and via Coulomb oscillation peak positions in transport through extremely small ($N \sim 0 - 30$) vertical quantum dots⁵³. Interestingly, a *classical* treatment, via Monte-Carlo molecular dynamics simulation⁵⁴ also predicts a shell structure. Here, the effect of the neutralizing positive background are assumed to produce a parabolic confining potential. A similar assumption is made in Ref.⁵⁵ which analyzes a vertical structure similar to that of Ref.⁵³. We believe that continued advances in fabrication will result in further emphasis on such invariant, as opposed to merely statistical, properties of dot spectra.

As noted above, there is a strong tendency for levels at the Fermi surface to “lock.” Such an effect has been

described by Sun *et al.*⁵⁶ in the case of subband levels for parallel quantum wires. In dots, the effect can be viewed as electrostatic pressure on the individual wavefunctions thereby shifting level energies in such a way as to produce level *occupancies* which minimize the total energy. Insofar as a given set of level occupancies is electrostatically most favorable, level locking is a temperature dependent effect which increases as T is lowered. This self-consistent modification of the level energies can also be viewed as an excitonic correction to excitation energies.

The difference between the cases of a quantum dot and that of parallel wires is one of localized versus extended systems. It is well known that, unlike Hartree-Fock theory, wherein self-interaction is completely cancelled since the direct and exchange terms have the same kernel $1/|\mathbf{r} - \mathbf{r}'|$, in Hartree theory and even density functional theory in the LDA, uncorrected self-interaction remains⁵⁷. While it is reasonable to expect that excited states will have their energies corrected downward by the remnants of an excitonic effect, we expect that LDA and especially Hartree calculations will generally overestimate this tendency to the extent that corrections for self-interaction are not complete.

The panel labelled “xc” in figure 9 illustrates the preceding point. In contrast to the large panel (on the left) these results have had the XC potential in LDA included. The differences between Hartree and LDA are generally subtle, but here the clustering of the levels at the Fermi surface is clearly mitigated by the inclusion of XC. The approximate parabolic degeneracy is evidently not broken by LDA, however, and the shell structure remains intact. Similarly for xc, the capacitances also show anomalies near the same gate voltages, where shells depopulate, as in figure 4, which is pure Hartree.

The two remaining panels in figure 9 illustrate the effects of disorder and ordering in the donor layer (XC not included). As with the “xc” panel, V_g is varied between -1.142 and -1.17 V. The “disorder” panel represents a single fixed distribution of ions placed at random in the donor layer as discussed above. Similarly, the “order” panel represents a single ordered distribution generated from a random distribution via the Monte-Carlo simulation^{6,21}; here $\mathcal{F} = 1/5$ (cf. two panels of Fig. 3).

The shell structure, which is completely destroyed for fully random donor placement (see also Fig. 14), is almost perfectly recovered in the ordered case. In both cases the energies are uniformly shifted upwards relative to the quiet dot by virtue of the discreteness of donor charge (cf. also discussion of Fig. 4 above). Closer examination of the disordered spectrum shows considerably more level repulsion than the other cases.

The application of a small magnetic field, roughly a single flux quantum through the dot, has a dramatic impact on both the spectrum, figure 13, and the wave functions, figure 14, top. The magnetic field dependence of the levels (not shown) up to 0.1 T exhibits shell splitting according to azimuthal quantum number as

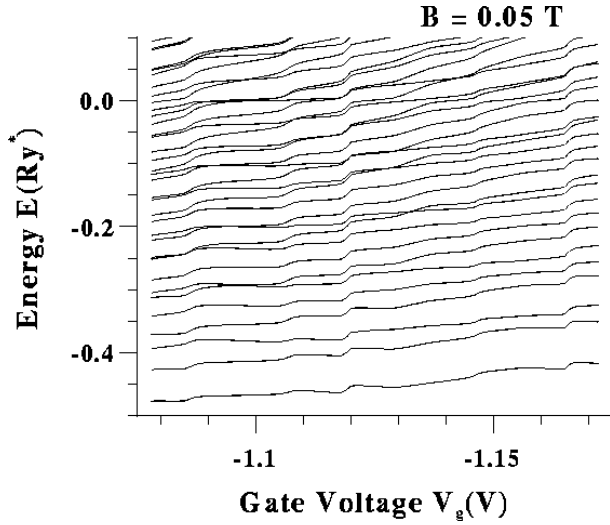


FIG. 13. V_g dependence at fixed B (0.05 T) of level energies, quiet dot. Multiple re-constructions seen as levels depopulate. Homogeneous level spacing related to uniformity of Coulomb oscillation peak heights in a magnetic field.

well as level anti-crossing. By 0.05 T level spacing (Fig. 13) is substantially more uniform than $B = 0$, Fig. 9. Furthermore, while the $B = 0$ quiet dot displays reconstruction due to the depopulation of shells at $V_g \approx -1.15$ and -1.1 V, the $B = 0.05$ T results show a similar pattern, a step in the levels, repeated

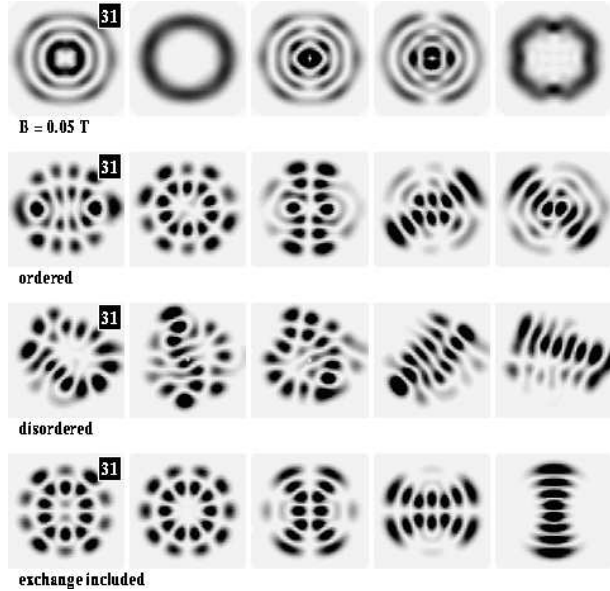


FIG. 14. Levels 31 through 35 for (from bottom) quiet dot with LDA for XC, Hartree for disordered dot, Hartree for ordered dot $\mathcal{F} = 1/5$ and $B = 0.05$ T. XC changes ordering of some levels, but has very little influence on states. Ordered case recovers much of quiet dot symmetry. Small B changes states altogether.

many times in the same gate voltage range. The physical meaning of this is clear. The magnetic field princi-

pally serves to remove the azimuthal dependence of the mod squared of the wave functions (Fig. 14). In a magnetic field, the states at the Fermi surface also tend to be at the dot perimeter. Depopulation of an electron in a magnetic field, like depopulation of the last member of a shell for $B = 0$, therefore removes charge from the perimeter of the dot and a self-consistent expansion of the remaining states outward occurs.

C. Statistical properties

1. Level spacings

The statistical spectral properties of quantum systems whose classical Hamiltonian is chaotic are believed to obey the predictions of random matrix theory (RMT)⁵⁸. Arguments for this conjecture however invariably treat the Hamiltonian as a large finite matrix with averaging taken only near the band center. Additionally, an often un-clearly stated assumption is that the system in question can be treated *semi-classically*, that is, in some sense the action is large on the scale of Planck's constant and the wavelength of *all relevant states* is short on the scale of the system size. Clearly, for small quantum dots these assumptions are violated.

RMT predictions apply to level spacings S and to transition amplitudes (for the “exterior problem,” level widths Γ)⁵⁹. RMT is also applied to scattering matrices in investigations of transport properties of quantum wires⁶⁰. Ergodicity for chaotic systems is the claim that variation of some external parameter X will sweep the Hamiltonian rapidly through its entire Hilbert space, whereupon energy averaging and ensemble (i.e. X) averaging produce identical statistics. In our study X is either the set of gate voltages, the magnetic field or the impurity configuration and we consider the statistics of the lowest lying 45 levels (spin is ignored here). Care must also be taken in removing the secular variations of the spacings or widths with energy, the so-called unfolding.

According to RMT level repulsion leads to statistics of level spacings which are given by the “Rayleigh distribution:”

$$P(S) = \frac{\pi S}{2D} \exp(-\pi S^2/4D^2) \quad (16)$$

where D is the mean local spacing^{59,61}. Figure 15 shows the calculated histogram for the level spacings for the quiet dot as well as for disordered, ordered and ordered with $B = 0.05$ T cases. Statistics are generated from (symmetrical) plunger gate variation, in steps of 0.001 V, over a range of 0.1 V, employing the spacings between the lowest 45 levels; thus about 4500 data points. Deviation from the Rayleigh distribution is evident. An important feature of our dot is symmetry under inversion through both axes bisecting the dot. It is well known that groups of states which are

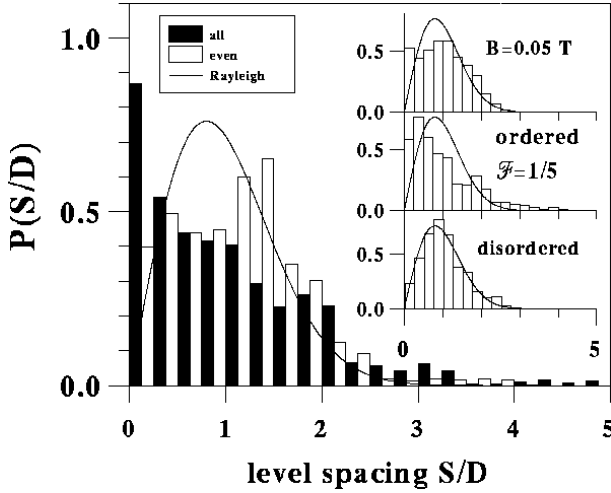


FIG. 15. Histograms of level spacings, normalized to local level spacing. Dark curve represents Rayleigh distribution. Black bars (main panel) include all states, white bars only for states that are completely even under x or y inversion. Insets: disordered panel recapitulates Rayleigh distribution, both ordered and $B \neq 0$ marginally but significantly different.

un-coupled will, when plotted together, show a Poisson distribution for the spacings rather than the level repulsion of Eq. 16. Thus we have also plotted (white bars) the statistics for those states which are totally even in parity. While the probability of degeneracy decreases, a χ^2 test shows that the distribution remains substantially removed from the Rayleigh form.

In contrast to this, the disordered case shows remarkable agreement with the RMT prediction. As with the spectrum in figure 9 we use a single ion distribution. However we also find (not shown) that fixing the gate voltage and varying the random ion distributions results in nearly the same statistics. When the ions are allowed to order the level statistics again deviate from the RMT model. This is somewhat surprising since Fig. 4 shows that, even for $\mathcal{F} = 1/5$, the standard deviation of the effective 2D potential below the Fermi surface from the quiet dot case, $\sim 0.05 Ry^*$, is still substantially greater than the mean level spacing $\sim 0.02 Ry^*$. We have recently shown that, as \mathcal{F} goes from unity to zero, a continuous transition from the level repulsion of Eq. 16 to a Poisson distribution of level spacings results⁶². Finally, the application of a magnetic field strong enough to break time-reversal symmetry clearly reduces the incidence of very small spacings, but the distribution is still significantly different from RMT.

2. Level widths

In Eq. 10 we defined $W_n(a, b)$ as the barrier penetration factor from the classically accessible region of the lead to the matching point in the barrier, for the n^{th} channel. The penetration factor *completely* through

the barrier, $P_n \equiv W_n(a, c)$ where c is the classical turning point on the dot side of the barrier, is plotted as a function of QPC voltage in figure 16. P_n is simply the WKB penetration for a given channel with a given self-consistent barrier profile, and can be computed at any energy. Here we have computed it at energies coincident with the dot levels. Therefore the dashes recapitulate the level structure, spaced now not in energy but in “bare” partial width. The *actual* width of a level depends upon the wave function for that state (cf. Eq. 10). For energies above the barrier $\ln(P) = 0$. The solid lines represent P at the Fermi surface computed for three different *AlGaAs* thicknesses t (as in figure 8) and for both $n = 1$ and $n = 2$ (the dashes are computed for $t = 12 a_B^*$). The QPC voltage is given relative to values at which P for $n = 1$ is the same for all three t (hence the top three solid lines converge at $\Delta V_{QPC} = 0$).

Quite surprisingly t has very little influence on the trend of P with QPC voltage. Note that the ratio of barrier penetration between the second and first channels P_2/P_1 decreases substantially with increasing t since the saddle profile becomes wider for more distant gates. Even for $t = 7.5 a_B^*$ however, penetration via the second channel is about a factor of five smaller than via $n = 1$.

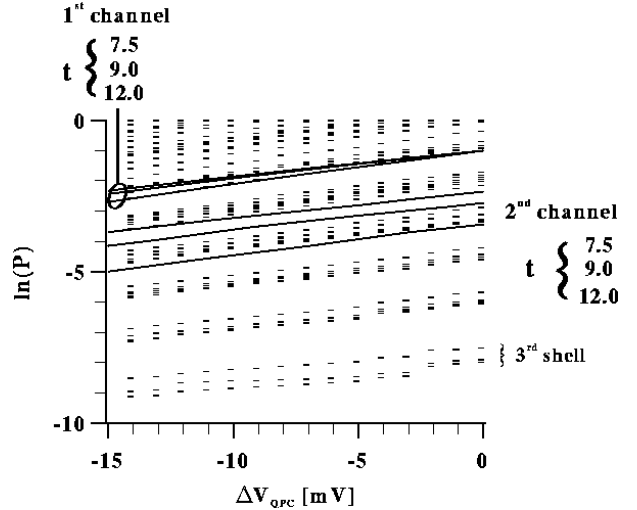


FIG. 16. Barrier penetration factors from classical turning point in lead to turning point in dot at same energy, as a function of QPC voltage offset. P evaluated at energies of states in quiet dot for *AlGaAs* thickness $t = 12 a_B^*$. Solid lines indicate barrier penetration at Fermi level. Upper three lines for first channel, $t = 7.5, 9.0, 12.0 a_B^*$ respectively. Lower three lines for second channel, same t . ΔV_{QPC} zero set such that first channel conducts equally at the Fermi surface for all t .

Figure 17 shows the partial width for tunneling via $n = 1$ through the barrier, now using the full Eq. 10, for the quiet dot. The barriers here are fairly wide. While this strikingly coherent structure is quickly destroyed by discretely localized donors even when donor ordering is allowed, the pattern is nonetheless highly informative.

The principal division between upper and lower states is based on parity. States which are odd with respect to the axis bisecting the QPC should in fact have identically zero partial width (that they don't is evidence of numerical error, mostly imperfect convergence).

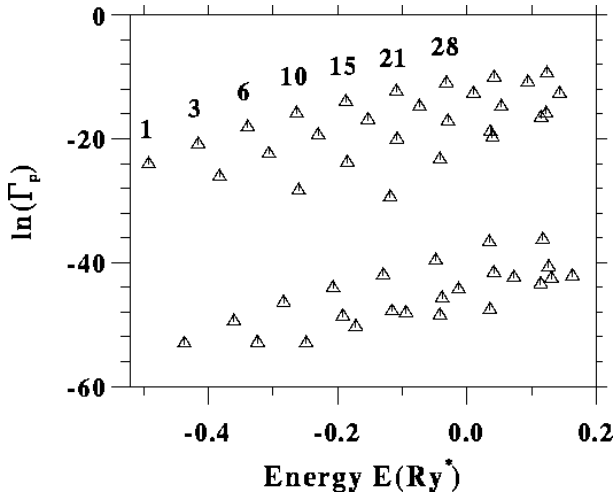


FIG. 17. Partial widths (through first channel) for tunneling to the leads, quiet dot. Numbers indicate ordinate of wave functions, Figs. 11 and 12. Weakly connected states zero by parity (non-zero only through numerical error).

Note that *this* division is largely preserved for discrete but ordered ions. The widest states (largest Γ) are labelled with their level index for comparison with their wave functions in Figs. 12 and 13. Comparison shows they represent the states which are aligned along the direction of current flow. Thus in each shell there are likely to be a spread of tunneling coefficients, that is, two members of the same shell will not have the same Γ .

Statistics of the level partial widths are shown in figure 18, here normalized to their local mean values. While the statistics for the quiet dot are in substantial disagreement with RMT it is clear that discreteness of the ion charge, even ordered, largely restores ergodicity. The RMT prediction, the ‘‘Porter-Thomas’’ (PT) distribution, is also plotted. For non-zero B , panels (b) and (c), the predicted distribution is χ^2_2 rather than PT. Even the completely disordered case (e) retains a fraction of vanishing partial width states. Since in our case the zero width states result from residual reflection symmetry, it would be interesting to compare the data from references⁶³ and⁶⁴, which employ nominally symmetric and non-symmetric dots respectively, to see if the incidence of zero width states shows a statistically significant difference.

One further statistical feature which we calculate is the autocorrelation function of the level widths as an external parameter X is varied:

$$C(\Delta X) = \frac{\sum_{i,j} \delta\Gamma_i(X_j) \delta\Gamma_i(X_j + \Delta X)}{\sqrt{\sum_{i,j} \delta\Gamma_i(X_j)^2} \sqrt{\sum_{i,j} \delta\Gamma_i(X_j + \Delta X)^2}} \quad (17)$$

where $\delta\Gamma_i(X) \equiv \Gamma_i(X) - \bar{\Gamma}_i(X)$, and where $\bar{\Gamma}(X)$ is again the *local* average, over levels at fixed X , of the level widths. Note that the sum on i is over levels and the sum on j is over starting values of X .

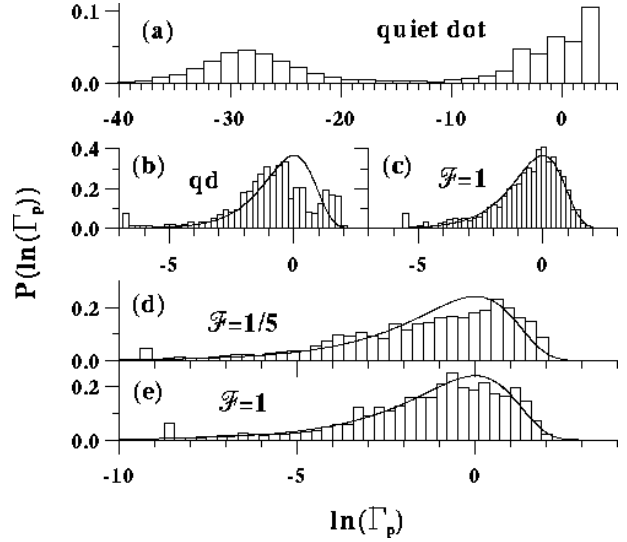


FIG. 18. Statistics of unfolded partial level widths, first channel only, (a) quiet dot showing large weight near zero due to parity, (b) and (c) have $B = 0.05 T$, quiet dot and disordered, respectively. Remnant of peak at small coupling remains. Dark line represents χ^2_2 distribution predicted by RMT. (d) and (e) are ordered and disordered with $B = 0$. Ordered case differs significantly from Porter-Thomas distribution plotted in black here.

In figure 19 we show the autocorrelation function for varying magnetic field (cf. Ref.⁶⁴, figure 3). The sample is ordered, $\mathcal{F} = 1/5$.

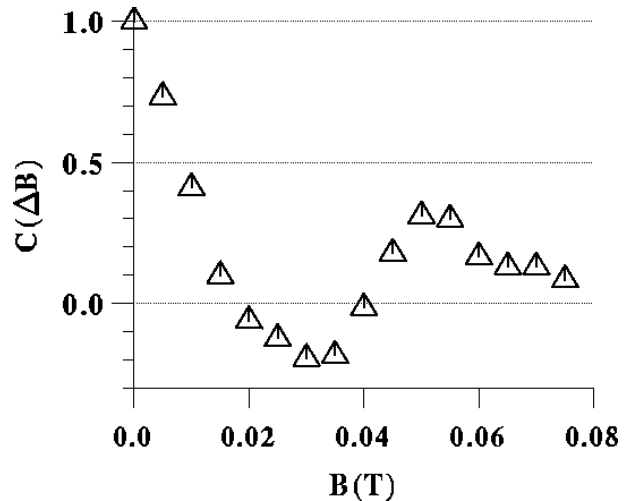


FIG. 19. Autocorrelation function for level partial widths; ordered, $\mathcal{F} = 1/5$, averaged over B starting point and all 45 levels. Range of B is only $0 - 0.1 T$, so statistics are weaker to the right. Pronounced anti-correlation near $0.03 T$ in contradiction with RMT.

Our range of B only encompasses $[0, 0.1]$ T in steps of 0.005 T , so we have here averaged over all levels (i.e. $i = 1 - 45$). The crucial feature, which has been noted in Refs.⁶⁴ and, for conductance correlation in open dots in⁶⁵, is that the correlation function becomes negative, in contradiction with a recent prediction based on RMT⁶⁶. Indeed, as noted by Bird *et al.*⁶⁵, an oscillatory structure seems to emerge in the data. Comparison with calculation here is hampered since the statistics are less good as B increases.

Nonetheless, the RMT prediction is clearly erroneous. We speculate that the basis of the discrepancy is in the assumption⁶⁶ that $C(\Delta X) = C(-\Delta X)$. Given this assumption⁶⁷ the correlation becomes positive definite. Physically this means that, regardless of whether B is positive or negative, the self-correlation of a level width will be independent of whether ΔB is positive or negative. This implies that the level widths should be independent of the absolute value of B , or any even powers of B , at least to lowest order in $\Delta B/B$. For real quantum dot systems this assumption is inapplicable.

Similar behaviour is observed with X taken as the (plunger) gate voltage, for which we have considerably more calculated results, Fig. 20.

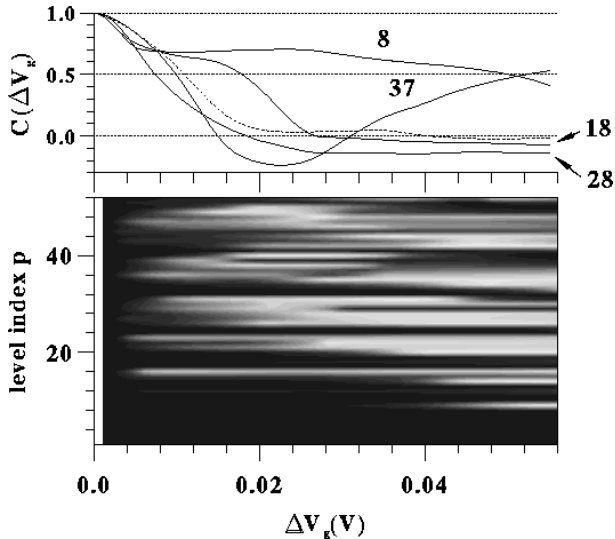


FIG. 20. Autocorrelation function with V_g , averaged over groups of 15 levels (upper panel). Number indicates center of (contiguous) range of averaged values. Dashed line is average of all states. Lower panel is grey scale for autocorrelation of individual levels averaged only over V_g starting point. Black is 1.0 and white is -1.0. Data suggests that behaviour of autocorrelation is sensitive to *which* levels are averaged.

The upper panel is the analogue of Fig. 19, only we have broken the average on levels into separate groups of fifteen levels centered on the level listed on the figure (e.g., the “28” denotes a sum in equ. 17 of $i = 21, 35$). the lower panel shows the autocorrelation as a grey scale for the individual levels (averaging performed only over starting V_g). The very low lying levels, up to ~ 10 , re-

main self-correlated across the entire range of gate voltage. This simply indicates that the correlation field is level dependent. However, rather than becoming uniformly grey in a Lorentzian fashion, as predicted by RMT⁶⁶, individual levels tend to be strongly correlated or anti-correlated with their original values, and the disappearance of correlation only occurs as an average over levels.

Again we expect that the explanation for this behaviour lies in the shell structure. Coulomb interaction prevents states which are nearby in energy from having common spatial distributions. Thus in a given range of energy, when one state is strongly connected to the leads, other states are less likely to be. Further, the ordering of states appears to survive at least a small amount of disorder in the ion configuration.

D. Conductance

The final topic we consider here is the Coulomb oscillation conductance of the dot. We will here focus on the temperature dependence⁴, although statistical properties related to ion ordering are also interesting.

We have shown in Ref.⁴ that detailed temperature dependence of Coulomb oscillation amplitudes can be employed as a form of quantum dot spectroscopy. Roughly, in the low T limit the peak heights give the individual level connection coefficients and, as temperature is raised activated conductance *at the peaks* depends on the nearest level spacings at the Fermi surface. In this regard we have explained envelope modulation of peak heights, which had previously not been understood, as clear evidence of thermal activation involving tunneling through excited states of the dot⁴.

Figure 21a shows the conductance as a function of plunger gate voltage for the ordered dot at $T = 250$ mK . Note that the magnitude of the conductance is small because the coupling coefficients are evaluated with relatively wide barriers for numerical reasons. Over this range the dot N depopulates from 62 (far left) to 39. The level spacings and tunneling coefficients are all changing with V_g . At low temperature a given peak height is determined mostly by the coupling to the first empty dot level (Γ_{N+1}) and by the spacings between the N^{th} level and the nearest other level (above or below). The relative importance of the Γ 's and the level spacings can obviously vary. In this example, Figs. 21a and 21b suggest that peak heights correlate more strongly with the level spacings. The double envelope coincides with the Fermi level passing through two shells. In general, the DOS fluctuations embodied in the shell structure and the observation (above) that within a shell a spreading of the Γ 's (with a most strongly coupled level) results from Coulomb interaction provide the two fundamental bases of envelope modulation.

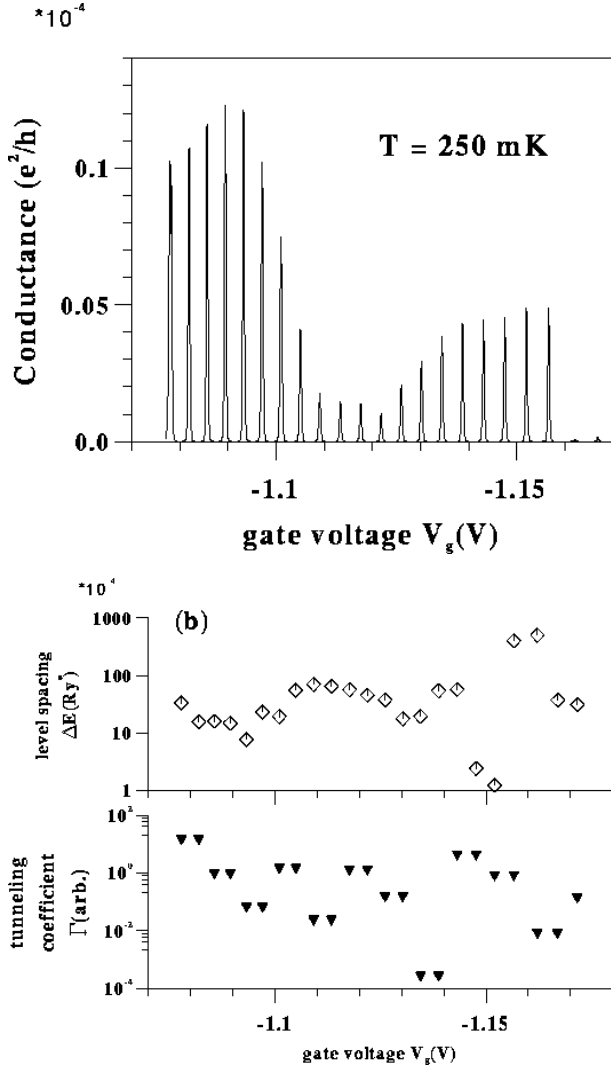


FIG. 21. (a) Conductance versus V_g for ordered dot, $T = 0.25$ K. (b) Fermi surface level spacing and tunneling coefficient at resonance. Conductance in (a) correlates somewhat more strongly with smaller level spacing than with larger Γ .

Finally, we typically find that, when peak heights are plotted as a function of temperature (not shown) some peaks retain activated conductance down to $T = 10$ mK. Since the dot which we are modelling is small on the scale of currently fabricated structures, this study suggests that claims to have reached the regime where all Coulomb oscillations represent tunneling through a single dot level are questionable.

IV. CONCLUSIONS

We have presented extensive data from calculations on the electronic structure of lateral $GaAs - AlGaAs$ quantum dots, with electron number in the range of $N = 50 - 100$. Among the principal conclusions which

we reach are the following.

The electrostatic profile of the dot is determined by metal gates at fixed voltage rather than a fixed space charge. As a consequence of this the model of the dot as a conducting disk with fixed, “external,” parabolic confinement is incorrect. Charge added to the dot resides much more at the dot perimeter than this model predicts.

The assumption of complete disorder in the donor layer is probably overly pessimistic. In such a case the 2DEG electrostatic profile is completely dominated by the ions and it is difficult to see how workable structures could be fabricated at all. The presence of even a small degree of ordering in the donor layer, which can be experimentally modified by a back gate, dramatically reduces potential fluctuations at the 2DEG level.

Dot energy levels show a shell structure which is robust to ordered donor layer ions, though for complete disorder it appears to break up. The shell structure is responsible for variations in the capacitance with gate voltage as well as envelope modulation of Coulomb oscillation peaks. The claims that Coulomb oscillation data through currently fabricated lateral quantum dots shows unambiguous transport through single levels are questionable, though some oscillations will saturate at a higher temperature than others.

The capacitance between the dot and a lead increases only very slightly as the QPC barrier is reduced. Thus the electrostatic energy between dot and leads is dominated by charge below the Fermi surface and splitting of oscillation peaks through double dot structures⁴⁹ is undoubtedly a result of tunneling.

Finally, chaos is well known to be mitigated in quantum systems where barrier penetration is non-negligible⁶⁸. Insofar as non-integrability of the underlying classical Hamiltonian is being used as the justification for an assumption of ergodicity⁶⁹ in quantum dots, our results suggest that further success in comparison with real (i.e. experimental) systems will occur only when account is taken in, for example, the level velocity^{66,70}, of the correlating influences of quantum mechanics.

ACKNOWLEDGMENTS

I wish to express my thanks for benefit I have gained in conversations with many colleagues. These include but are not limited to: Arvind Kumar, S. Das Sarma, Frank Stern, J. P. Bird, Crispin Barnes, Yasuhiro Tokura, B. I. Halperin, Catherine Crouch, R. M. Westervelt, Holger F. Hofmann, Y. Aoyagi, K. K. Likharev, C. Marcus and D. K. Ferry. I am also grateful for support from T. Sugano, Y. Horikoshi, and S. Tarucha. Computational support from the Fujitsu VPP500 Supercomputer and the Riken Computer Center is also gratefully acknowledged.

- ¹ For a review see, D. Averin and K. K. Likharev, in: *Mesoscopic Phenomena in Solids* edited by B. L. Altshuler, P. A. Lee and R. A. Webb, Elsevier, Amsterdam, (1990).
- ² D.V. Averin, A.N. Korotkov, K.K. Likharev, Phys. Rev. B **44**, 6199, (1991).
- ³ C.W.J. Beenakker, Phys. Rev. B **44**, 1646 (1991).
- ⁴ A short paper concerning these results has already appeared in: M. Stopa, Phys. Rev. B **48**, 18340 (1993).
- ⁵ M. Stopa, to be published.
- ⁶ M. Stopa, Phys. Rev. B **53**, 9595 (1996).
- ⁷ F. Stern and S. Das Sarma, Phys. Rev. B **30**, 840 (1984).
- ⁸ J. C. Slater, *The Self-Consistent Field for Molecules and Solids*, McGraw-Hill, New York, 1974.
- ⁹ M. Stopa, J. P. Bird, K. Ishibashi, Y. Aoyagi and T. Sugano, Phys. Rev. Lett. **76**, (1996).
- ¹⁰ A. Kumar, S. Laux and F. Stern, Phys. Rev. B **42**, 5166 (1990).
- ¹¹ T. Ando, A. Fowler and F. Stern, Rev. Mod. Phys. **54**, 437 (1982).
- ¹² For a discussion of the treatment of surface states see: J. H. Davies and I. A. Larkin, Phys. Rev. B **49**, 4800 (1994); J. H. Davies, Semicond. Sci. Technol. **3**, 995 (1988).
- ¹³ J. A. Nixon and J. H. Davies, Phys. Rev. B **41**, 7929 (1990).
- ¹⁴ Recently, G. Pilling, D. H. Cobden, P. L. McEuen, C. I. Duruöz and J. S. Harris Jr., *Proceedings of the Eleventh International Conference on the Electronic Properties of Two Dimensional Systems*, Surface Science (in press), have presented experimental evidence of electrons escaping from the 2DEG layer into the substrate upon tunneling beneath a barrier.
- ¹⁵ Studies of edge states in quantum Hall liquids, for example, uniformly assume perfectly 2D systems, see for example C. de C. Chamon and X. G. Wen, Phys. Rev. B **49**, 8227 (1994).
- ¹⁶ D. Jovanovic and J. P. Leburton, Phys. Rev. B, **49**, 7474 (1994).
- ¹⁷ C. G. Darwin, Proc. Cambridge Philos. Soc. **27**, 86 (1931).
- ¹⁸ R. E. Bank and D. J. Rose, SIAM J. Numer. Anal., **17**, 806 (1980).
- ¹⁹ E. Buks, M. Heiblum and Hadas Shtrikman, Phys. Rev. B **49**, 14790 (1994); P. Sobkowicz, Z. Wilamowski and J. Kossut, Semicond. Sci. Technol. **7**, 1155 (1992).
- ²⁰ A. L. Efros, Solid State Comm. **65**, 1281 (1988); T. Suski, P. Wisniewski, I. Gorczyca, L. H. Dmowski, R. Piotrkowski, P. Sobkowicz, J. Smoliner, E. Gornik, G. Böm and G. Weimann, Phys. Rev. B **50**, 2723 (1994).
- ²¹ Y. Aoyagi, M. Stopa, H. F. Hofmann and T. Sugano, in *Quantum Coherence and Decoherence*, edited by K. Fujikawa and Y. A. Ono, Elsevier, Holland (1996).
- ²² J. P. Bird, K. Ishibashi, M. Stopa, R. P. Taylor, Y. Aoyagi and T. Sugano, Phys. Rev. B **49**, 11488 (1994).
- ²³ H. van Houten, C.W.J. Beenakker, A.A.M. Staring in *Single Charge Tunneling*, edited by H. Grabert and M.H. Devoret, NATO ASI Series B (Plenum, New York, 1991).
- ²⁴ Y. Meir, N. Wingreen, P.A. Lee, Phys. Rev. Lett. **66**, 3048 (1991).
- ²⁵ J. Bardeen, Phys. Rev. Lett. **6**, 57 (1961).
- ²⁶ K. A. Matveev, Phys. Rev. B **51**, 1743 (1995).
- ²⁷ J. H. F. Scott-Thomas, S. B. Field, M. A. Kastner, D. A. Antoniadis and H. I. Smith, Phys. Rev. Lett. **62**, 583 (1989); U. Meirav, M. A. Kastner and S. J. Wind, Phys. Rev. Lett. **65**, 771 (1990); L.P. Kouwenhoven, N.C. van der Vaart, A.T. Johnson, C.J.P.M. Harmans, J.G. Williamson, A.A.M. Staring, C.T. Foxon, proceedings of the German Physical Society meeting, Münster 1991; Festkörperprobleme/Advances in Solid State Physics (Volume 31); E. B. Foxman, P. L. McEuen, U. Meirav, N. Wingreen, Y. Meir, P. A. Belk, N. R. Belk, M. A. Kastner and S. J. Wind, Phys. Rev. B **47**, 10020 (1993).
- ²⁸ M. Stopa, Y. Aoyagi and T. Sugano, Phys. Rev. B, **51**, 5494 (1995).
- ²⁹ M. Stopa and Y. Tokura, in *Science and Technology of Mesoscopic Structures*, edited by S. Namba, C. Hamaguchi and T. Ando, Springer-Verlag, Tokyo, (1992).
- ³⁰ M. Büttiker, J. Phys. Condens. Matter **5**, 9361 (1993).
- ³¹ P. Hohenberg and W. Kohn, Phys. Rev. **136** B864 (1964).
- ³² W. Kohn and L. Sham, Phys. Rev. **140** A1133 (1965).
- ³³ P. L. McEuen, E. B. Foxman, U. Meirav, M. A. Kastner, Y. Meir, N. S. Wingreen and S. J. Wind, Phys. Rev. Lett. **66**, 1926 (1991).
- ³⁴ R. C. Ashoori, H. L. Stormer, J. S. Weiner, L. N. Pfeiffer, S. J. Pearton, K. W. Baldwin and K. W. West, Phys. Rev. Lett. **68**, 3088 (1992).
- ³⁵ R. Jalabert, H.U. Baranger and A. D. Stone, Phys. Rev. Lett. **65**, 2442 (1990).
- ³⁶ C. W. J. Beenakker and H. van Houten, Phys. Rev. Lett. **63**, 1857 (1989).
- ³⁷ J. P. Bird, D. M. Olatona, R. Newbury, R. P. Taylor, K. Ishibashi, M. Stopa, Y. Aoyagi, T. Sugano and Y. Ochiai, Phys. Rev. B **52**, R14336 (1995).
- ³⁸ D. K. Ferry and G. Edwards, preprint.
- ³⁹ In other words, since the dot floor is not flat, even a lithographically square dot, say, with gates very close to the 2DEG plane would seem to suffer rounding of the resulting potential departing appreciably from the flat bottomed, hard walled square shape envisioned.
- ⁴⁰ P. M. Mooney, J. Appl. Phys. **67**, R1 (1990).
- ⁴¹ E. Yamaguchi, K. Shiraishi and T. Ono, Jour. Phys. Soc. Jap. **60**, 3093 (1991).
- ⁴² M. Heiblum, private communication.
- ⁴³ M. Stopa, Y. Aoyagi and T. Sugano, Surf. Sci. **305**, 571 (1994).
- ⁴⁴ V. Shikin, S. Nazin, D. Heitmann and T. Demel, Phys. Rev. B **43**, 11903 (1991); S. Nazin, K. Tevosyan and V. Shikin, Surf. Sci. **263**, 351 (1992).
- ⁴⁵ D. B. Chklovskii, B. I. Shklovskii and L. I. Glazman, Phys. Rev. B **46**, 15606 (1992).
- ⁴⁶ K. A. Matveev, preprint.
- ⁴⁷ J. Golden and B. I. Halperin, preprint.
- ⁴⁸ H. Yi and C. L. Kane, Report No. cond-mat/9500139.
- ⁴⁹ F. R. Waugh, M. J. Berry, D. J. Mar, R. M. Westervelt, K. L. Campman and A. C. Gossard, Phys. Rev. Lett. **75**, 705 (1995).
- ⁵⁰ I. M. Ruzin, V. Chandrasekhar, E. I. Levin and L. I. Glazman, Phys. Rev. B **45**, 13469 (1992).
- ⁵¹ See M. Stopa and S. Das Sarma, Phys. Rev. B **47**, 2122 (1993), and references therein.
- ⁵² D. J. Lockwood, P. Hawrylak, P. D. Wang, C. M. Sotomayor Torres, A. Pinczuk and B. S. Dennis, Phys. Rev. Lett. **77**, 354 (1996).

- ⁵³ S. Tarucha, D. G. Austing, T. Honda, R. J. van der Hage and L. P. Kouwenhoven (to be published).
- ⁵⁴ F. M. Peeters, V. A. Schweigert and V. M. Bedanov, *Physica B* **212**, 237 (1995).
- ⁵⁵ Y. Tanaka and H. Aker, *Phys. Rev. B* **53**, 3901 (1996).
- ⁵⁶ Y. Sun and G. Kirczenow, *Phys. Rev. Lett.* **72**, 2450 (1994).
- ⁵⁷ For a discussion of corrections to self-interaction in density functional calculations, see: J. P. Perdew and A. Zunger, *Phys. Rev. B* **23**, 5048 (1981).
- ⁵⁸ A. V. Andreev, O. Agam, B. D. Simons and B. L. Altshuler, *Phys. Rev. Lett.* **76**, 3947 (1996).
- ⁵⁹ T. A. Brody, J. Flores, J. B. French, P. A. Mello, A. Pandey and S. S. M. Wong, *Rev. Mod. Phys.* **53**, 385 (1981).
- ⁶⁰ See K. Slevin and T. Nagao, *International Jour. Mod. Phys. B* **9**, 103 (1995), and references therein.
- ⁶¹ E. P. Wigner, in *Conference on Neutron Physics by Time-of-Flight*, Gatlinburg, Tennessee, 1956 (ORNL-2309, Oak Ridge National Laboratory).
- ⁶² M. Stopa, *Microstructures and Superlattices* (in press).
- ⁶³ A. M. Chang, H. U. Baranger, L. N. Pfeiffer, K. W. West and T. Y. Chang, *Phys. Rev. Lett.* **76**, 1695 (1996).
- ⁶⁴ J. A. Folk, S. R. Patel, S. F. Godijn, A. G. Huibers, S. M. Cronenwett, C. M. Marcus, K. Campman and A. C. Gossard, *Phys. Rev. Lett.* **76**, 1699 (1996).
- ⁶⁵ J. P. Bird, K. Ishibashi, Y. Aoyagi, T. Sugano and Y. Ochiai, *Phys. Rev. B* **50**, 18678 (1994).
- ⁶⁶ Y. Alhassid and H. Attias, *Phys. Rev. Lett.* **76**, 1711 (1996).
- ⁶⁷ I am indebted to Dr. David Ferry for an informative discussion on this point.
- ⁶⁸ U. Smilansky, in *Proceedings of the 1994 Les-Houches Summer School on "Mesoscopic Quantum Physics"*, ed. by E. Akkermans, G. Montambaux and J. L. Pichard (in press).
- ⁶⁹ R. A. Jalabert, A. D. Stone, and Y. Alhassid, *Phys. Rev. Lett.* **68**, 3468 (1992).
- ⁷⁰ B. D. Simons and B. L. Altshuler, *Phys. Rev. B* **48**, 5422 (1993).